Electronic Supplementary Material (ESI) for Journal of Materials Chemistry A.

Supplementary Information

Core-shell MnO_2@Au Nanofibers Network as High-Performance Flexible Transparent Supercapacitor Electrode

Soram Bobby Singh[a], Thangjam Ibomcha Singh[a], Nam Hoon Kim[a], Joong Hee Lee[a, b,*]

[a]*Advanced Materials Institute of BIN Convergence Technology (BK21 plus Global) and Department of BIN Convergence Technology, Chonbuk National University, Jeonju, Jeonbuk, 54896, Republic of Korea*

[b]*Carbon Composite Research Centre, Department of Polymer-Nano Science and Technology, Chonbuk National University, Jeonju, Jeonbuk 54896, Republic of Korea.*

**Corresponding author: e-Mail: jhl@chonbuk.ac.kr (Joong Hee Lee)*

Supplementary Figures

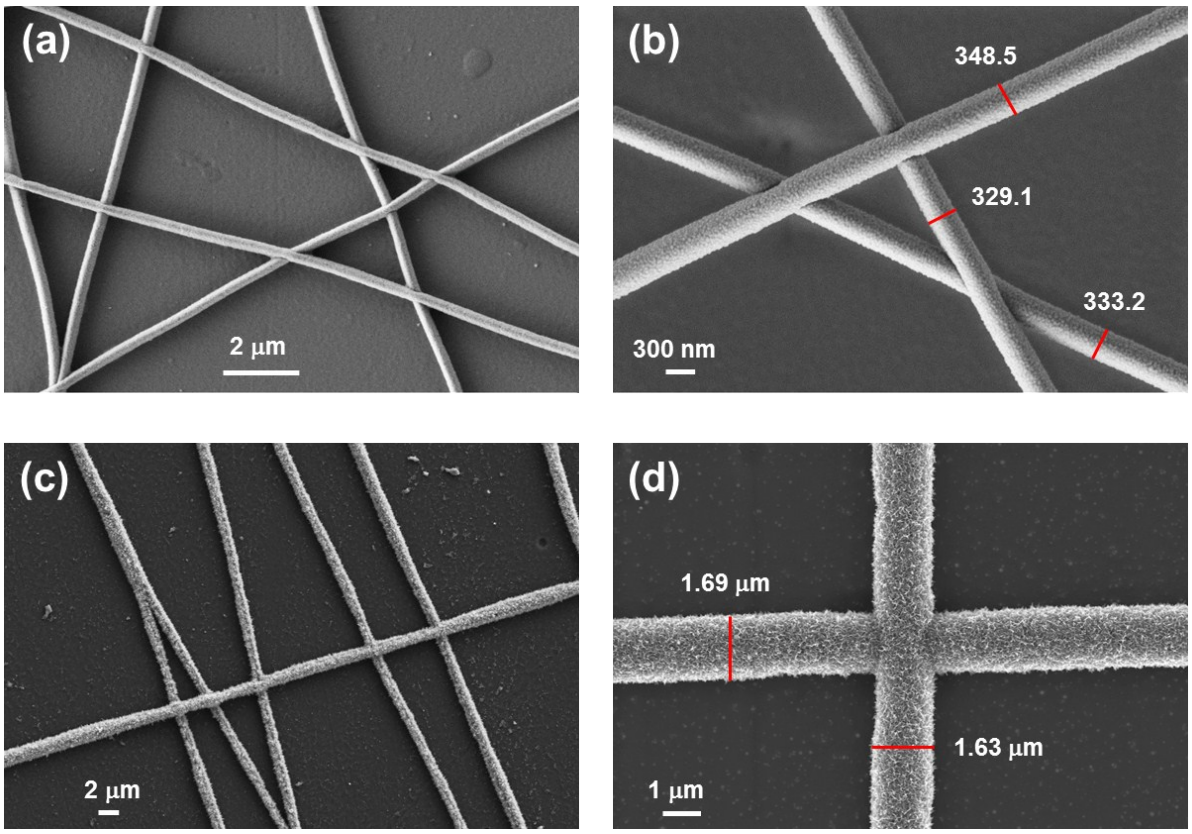

Fig. S1 (a) FE-SEM photograph of gold coated PVA nanofiber network. (b) Magnified FE-SEM photograph of (a), showing junctionless nanofiber structure with an average nanofiber diameter of ~330 nm. (c) FE-SEM photograph of electrodeposited MnO_2@AuNFs network electrode (9 min). (d) Magnified FE-SEM of (c) demonstrating a fused MnO_2@AuNFs network structure with an average diameter of ~1.6 μm.

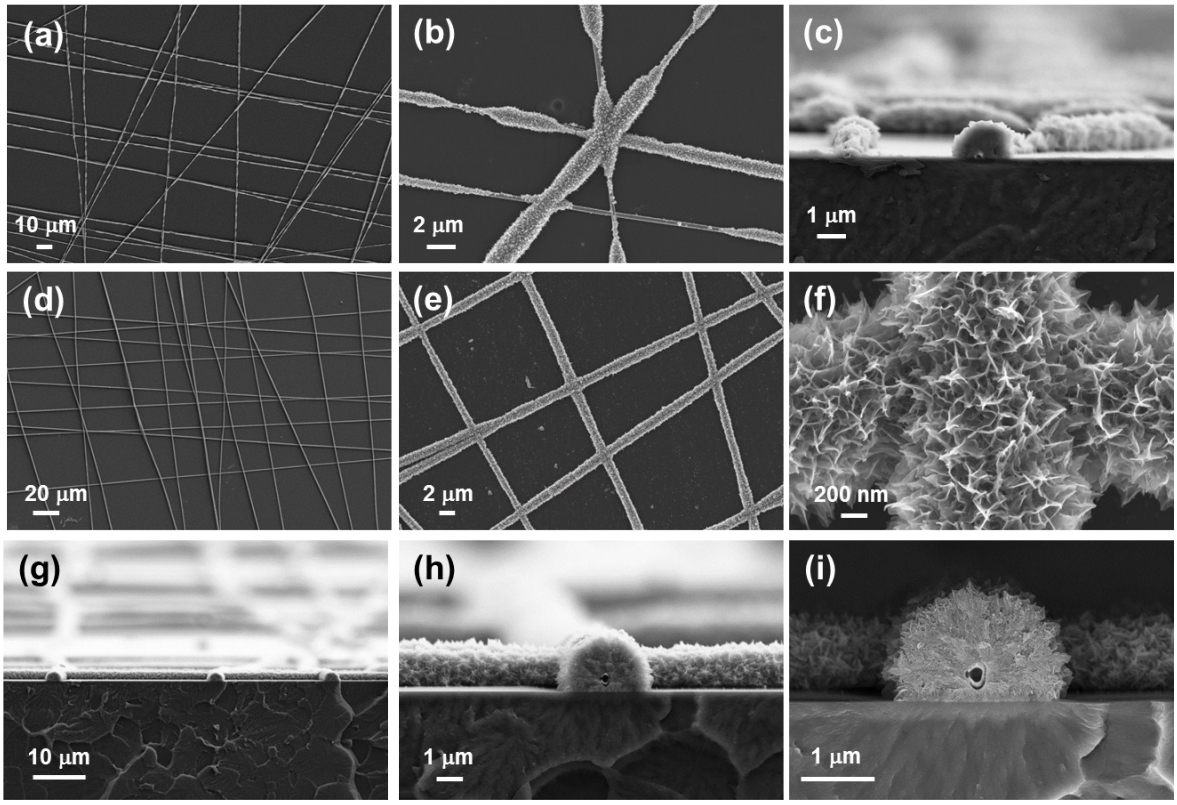

Fig. S2 FE-SEM photograph of MnO_2@AuNFs network electrode on PEN substrates at different electrodeposition time: (a, b) low and magnified FE-SEM of 3 min electrodeposition time MnO_2 electrode showing non-uniform coating of MnO_2 over the AuNFs network electrode. (c) Cross-sectional magnified FE-SEM photograph of (a), (d, e) low and magnified FE-SEM photograph of 9 min electrodeposition time suggesting a uniform coating of MnO_2 over the AuNFs network. (f) Magnified FE-SEM photograph of (e), showing spicky nanosheet MnO_2 morphology. (g-i) Cross-sectional FE-SEM image at different magnification confirming the formation of core-shell MnO_2@AuNFs network electrode structure.

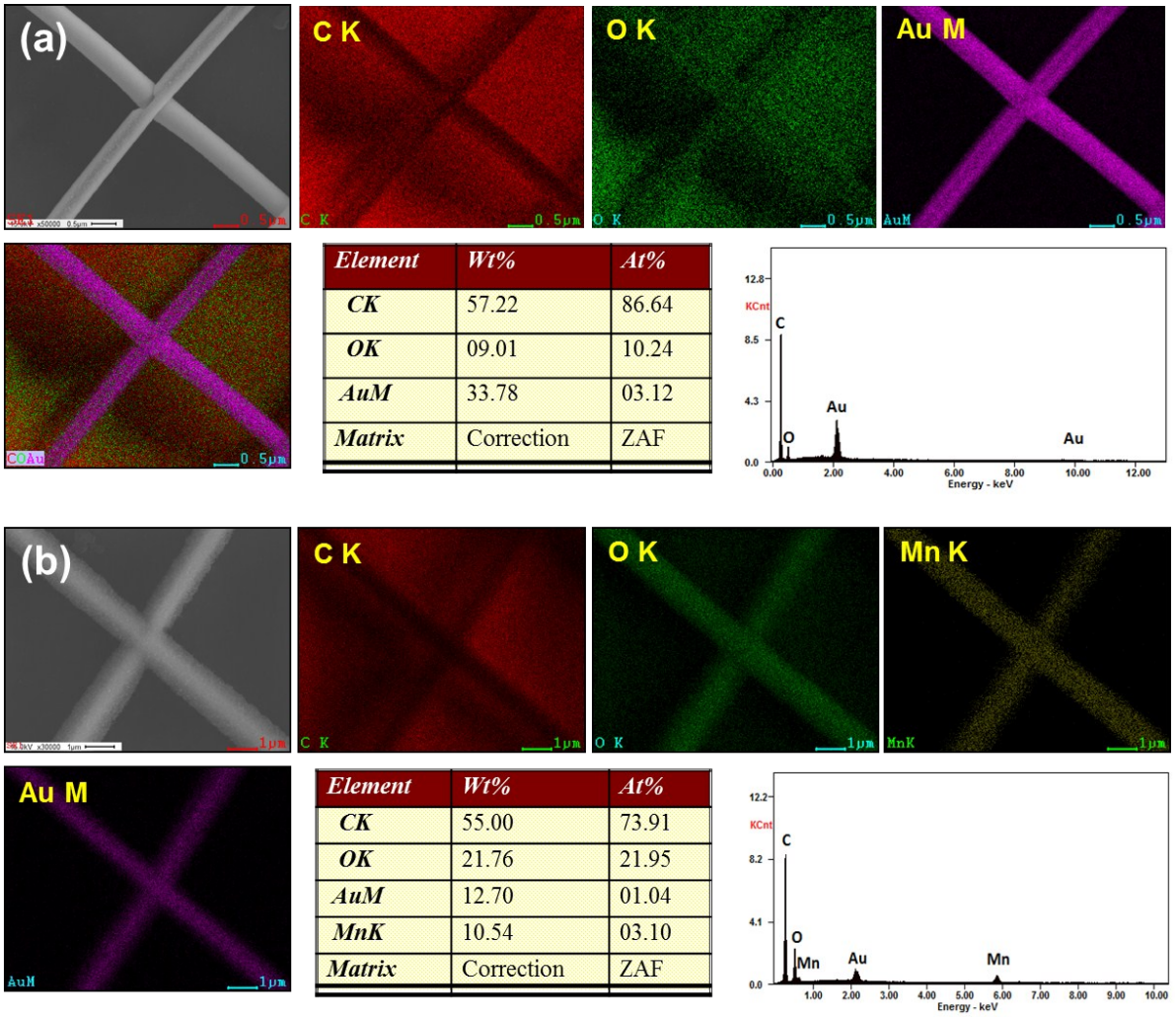

Fig. S3 Elemental analysis of bare AuNFs and electrodeposited MnO_2@AuNFs network electrode on PEN substrates. EDS mapping of (a) AuNFs network electrode before MnO_2 electrodeposition and (b) after MnO_2 electrodeposition (9 min).

From the EDS mapping analysis Figure S2 (a), it is quite confirmed that gold is uniformly coated over the PVA nanofiber template by thermal deposition. Again, Figure S2 (b) EDS mapping image of MnO_2@AuNFs network (9 min) shows the uniform distribution of Mn, O, and Au elements throughout the whole AuNFs area.

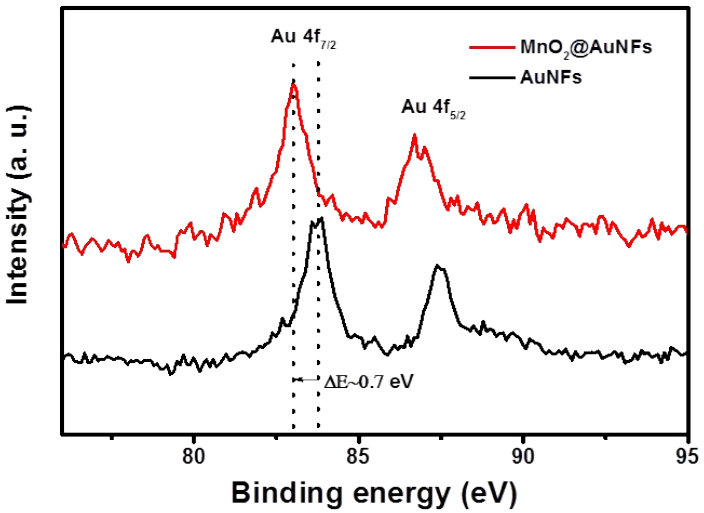

Fig. S4 Comparison of Au 4f binding energy of the bare AuNFs network electrode and MnO_2@AuNFs network electrode after electrodeposition. A red shift in the binding energy is clearly observed suggesting a strong interaction between core AuNFs and shell MnO_2 nanosheet.

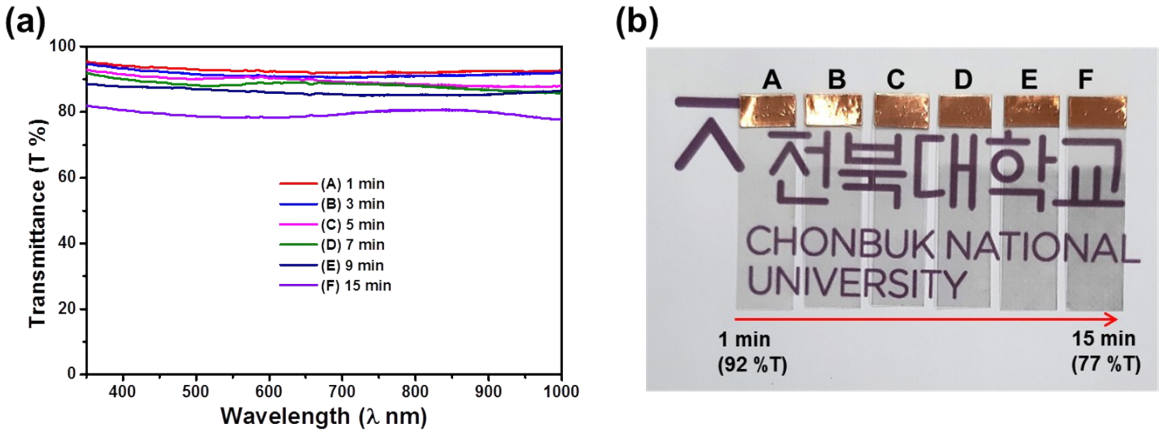

Fig. S5 (a) Optical transmittance spectra of electrodeposited MnO_2@AuNFs network electrode for different electrodeposition time. (b) Digital photographs of MnO_2@AuNFs electrode on PEN substrate at different electrodeposition time.

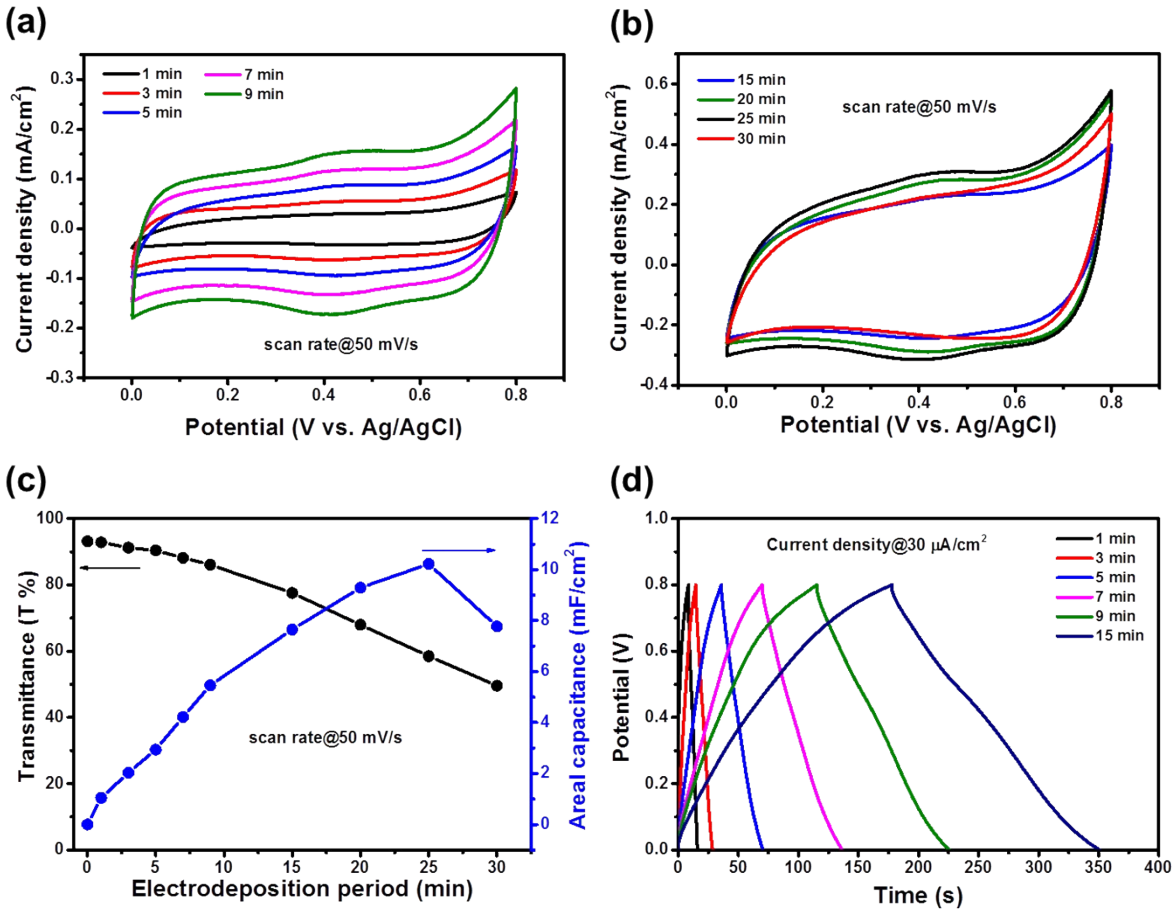

Fig. S6 Electrochemical measurements of the core-shell MnO_2@AuNFs network electrode in a three-electrode configuration in 1 M Na_2SO_4 electrolyte. (a, b) Cyclic voltammograms (CVs) of the electrode with different MnO_2 electrodeposition times at a scan rate of 50 mV/s. (c) Optical transmittance and areal capacitance as a function of MnO_2 electrodeposition time (areal capacitance derived from Fig S5a,b). (d) Cyclic voltammograms (CVs) of the electrode with different MnO_2 electrodeposition times at a scan rate of 50 mV/s. GCD curves of the MnO_2@AuNFs/PEN electrodes for different MnO_2 electrodeposition time at a current density of 30 $\mu A/cm^2$.

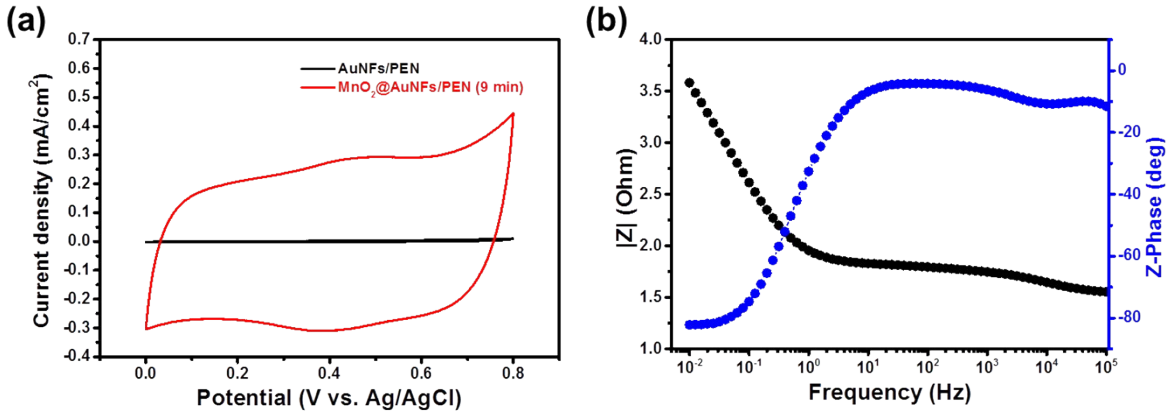

Fig. S7 (a) Comparison of the CV curves of bare AuNFs/PEN electrode with 9 min electrodeposited MnO_2@AuNFs/PEN electrode at a scan rate of 100 mV/s. (b) Bode plot, frequency dependent impedance, and phase angles of the MnO_2@AuNFs network electrode in the frequency range of 0.01 to 100 kHz.

Calculation of Areal capacitances and Energy densities

In the case of the three-electrode configuration system, the areal capacitance (mF/cm^2) of the film was derived from the 5th cycle of each CV scan using the following Equation (1)

$$C/A = \frac{1}{\nu A(V_f - V_i)} \int_{V_i}^{V_f} j dV \qquad (1)$$

where *A* is the effective area of the electrode film (*A*=2x1 cm^2)

In the case of the two-electrode configuration system, the areal capacitance of the device was calculated based on the area of the device as according to the following Equation (2)

$$C_{device}^{areal} = \frac{1}{\nu A_{device}(V_f - V_i)} \int_{V_i}^{V_f} j dV \qquad (2)$$

where C_{device}^{areal} (in F/cm^2) refer to the areal capacitance of the device and A_{device} is the total area (cm^2) of the conducting electrodes in the device, respectively.

The C/A (in F/cm^2) was also calculated from the galvanostatic charge/discharge (GCD) curves using Equation (3)

$$C/A = \frac{I}{A \times (dV/dt)} \qquad (3)$$

where *I* is the discharge current (A), *A* is the total area of the electrodes (cm^2), and dV/dt is the slope of the galvanostatic discharge curve.

Energy densities and power densities were calculated using Equation (4) as follows

$$E = \frac{C \times (\Delta V)^2}{2 \times 3600} \quad (4a)$$

$$P = \frac{E}{\Delta t \times 3600} \quad (4b)$$

Where E is the energy density (Wh/cm^2), C is the areal capacitance (F/cm^2), ΔV is the discharge voltage range (V) and Δt is the discharge time (s)

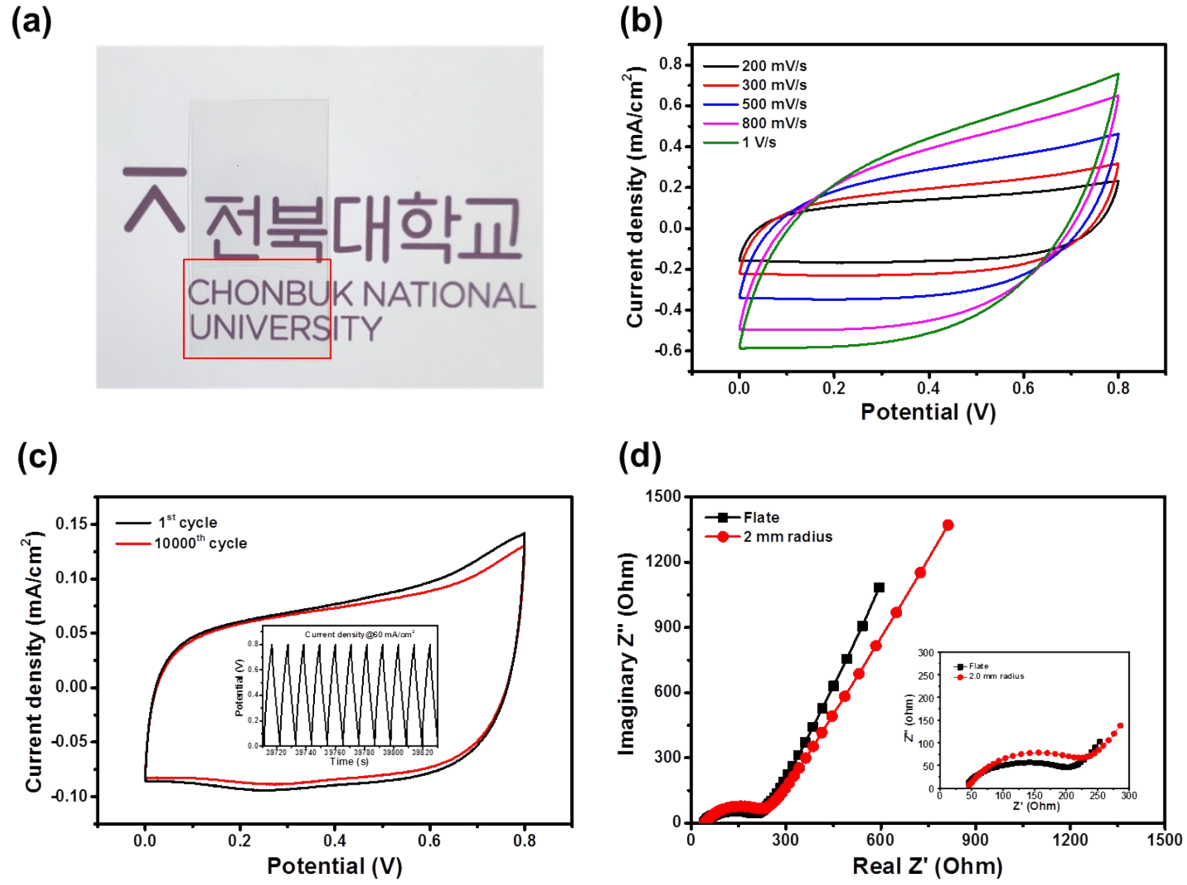

Fig. S8 (a) Digital photograph of PVA/LiCl gel film coated on a PEN substrate showing its high transparency (gel film: area under red mark). (b) CV curves of MnO_2@AuNFs network electrode (9 min) at different scan rate from 200 mV/s to 1 V/s. (c) Comparison of the CV curves of the device at 1st and 10,000th charge/discharge cycles showing almost 95% retention. (d) Nyquist plot for the supercapacitor devices before and after bending to a radius of 2 mm in the frequency range of (0.1 to 100) kHz.

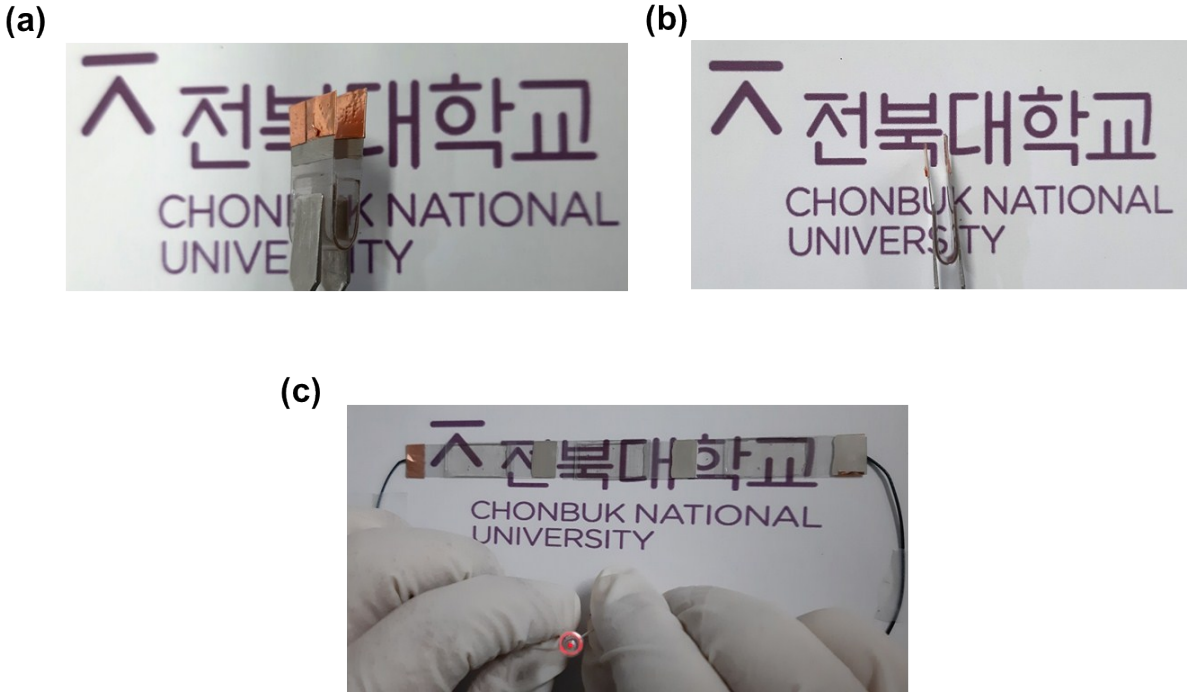

Fig. S9 (a and b) Digital photographs of a flexible transparent supercapacitor device showing its high bending capability. (c) Digital photograph of a RED LED lamp (1.8 V) powered by three devices connected in a series configuration.

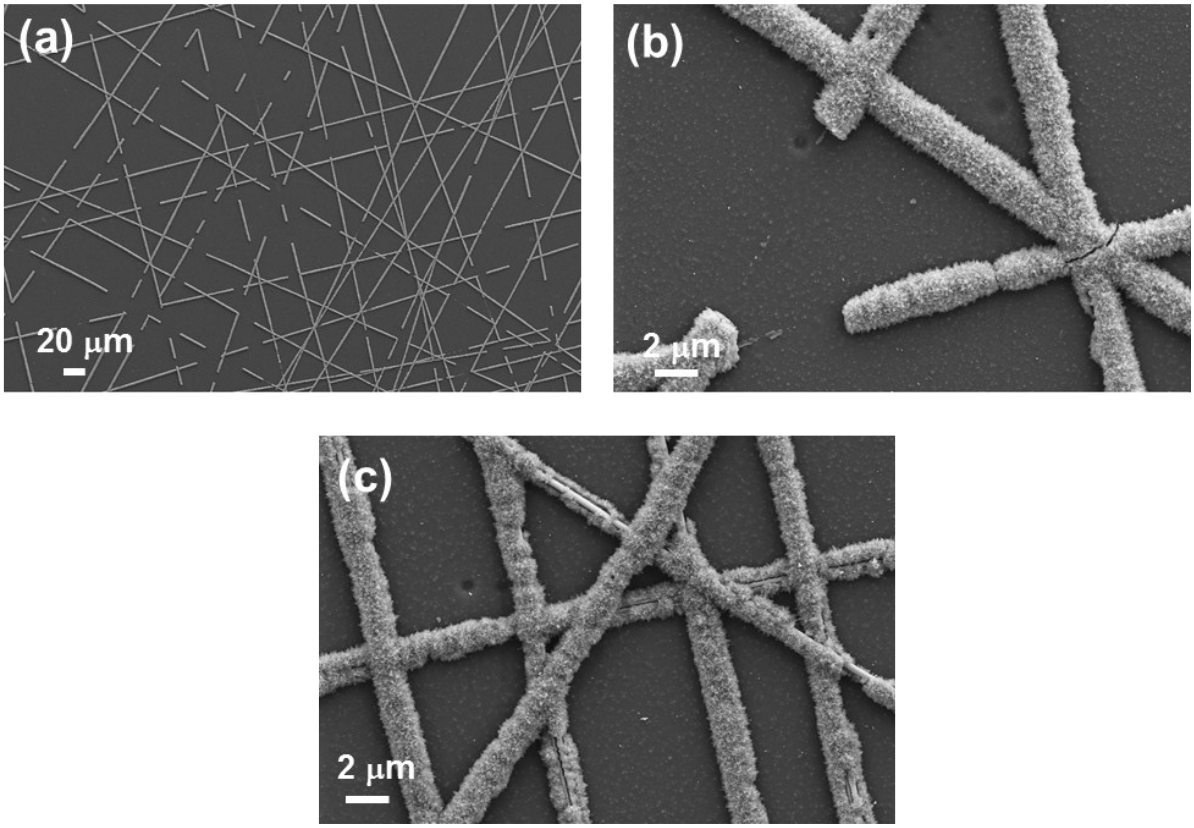

Fig. S10 (a)Low magnification, (b,c) high magnifications FE-SEM photographs of MnO_2@AuNFs network electrode on a PEN substrate, after sonication for 10 min using a 8200H MUJI Ultrasonicator at a frequency of 28 kHz.

It is clearly observed that some MnO_2@AuNFs were broken at few places of the network and detachment of MnO_2 nanosheets from the core AuNFs were observed in some areas of the network indicating the instability of MnO_2@AuNFs network electrode under ultrasonication.

Table S1. A comparative table showing the areal capacitance and transparency of present work with earlier reported transparent supercapacitors.

Material	**C/A (mF/cm^2)**	**Transmittance (T%)**	**Reference**
CNF-RGO	1.730	30	[1]
Graphene	0.101	75	[2]
Nanocups	0.409	71	[3]
SWCNT	0.584	60	[4]
Au@MnO_2 supercapacitor device	0.795	36	[5]
Graphene	3.3	47	[6]
PEDOT:PSS	1.18	65	[7]
Au/MnO_2 network	3.23	~76	[8]
GNHC-GF	5.48	44	[9]
Ag/Au/PPy	0.58	64	[10]
RuO_2/PEDOT supercapacitor device	0.84	80	[11]
Graphene Q-dot	0.009	93	[12]
$Ti_3C_2T_x$	0.87	80	[13]
Embedded Ag Grid electrode	2.79	~81	[14]
Embedded Ni mesh/PEDOT:PSS	0.52	83	[15]
PEDOT:PSS/Ag grid electrodes	2.84	-	[16]
MnO_2@Ni (supercapacitor device)	10.6	~80	[17]
PEDOT:PSS/AgNWs	0.6	~51	[18]
HTSE film	3.64	~85	[19]
ITO/Co_3O_4	6.03	51	[20]
In_2O_3/SWCNT In sphere	0.81	79	[21]
MnO_2/ITO/PET	4.73	44	[22]
AgNWs/NiOH/PEDOT:PSS	3.45	86	[23]
ITO/Ni@Gr-TF/Fe@Gr-TF	10.9	51	[24]
Ag NW/rGO/PANI	6.4	57	[25]
MnO_2@AuNFs	**8.26**	**86**	**This work**
MnO_2@AuNFs supercapacitor device	**2.07**	**79**	**This work**

Table S2. Summary of energy densities and power densities in of our device in comparison with previously reported transparent supercapacitor device.

Active material	Power density ($\mu W/cm^2$)	Energy density ($\mu Wh/cm^2$)	Ref
$Ti_3C_2T_x$ (symmetric)	0.62	0.049	[13]
	1.24	0.034	
	2.51	0.025	
	5.14	0.02	
	10.91	0.018	
PEDOT:PSS	1.16	0.009	[11]
	1.82	0.008	
	3.7	0.008	
	11.76	0.0079	
	20.92	0.006	
Ruo_2/PEDOT:PSS	0.28	0.015	[11]
	1.13	0.014	
	2.08	0.014	
	4.83	0.014	
	19.47	0.011	
Graphene Qdot	0.094	0.00079	[12]
	0.083	0.00082	
	0.072	0.00084	
	0.062	0.00087	
RMGO	9	0.014	[26]
Ag NW/$Ni(OH)_2$-PEIE/PEDOT:PSS	3.2	0.074	[23]
	4	0.072	
	6	0.069	
	12	0.059	
	20	0.05	
MnO_2@AuNFs	**4**	**0.143**	**This work**
	8	**0.101**	
	12	**0.078**	
	16	**0.066**	
	20	**0.054**	

Reference

1 K. Gao, Z. Shao, X. Wu, X. Wang, Y. Zhang, W. Wang, F. Wang, *Nanoscale*, 2013, **5**, 5307.

2 K. Jo, S. Lee, S. M. Kim, J. B. In, S. M. Lee, J. H. Kim, H. J. Lee, K. S. Kim, *Chem. Mater.*, 2015, **27**, 3621.

3 H. Y. Jung, M. B. Karimi, M. G. Hahm, P. M. Ajayan, Y. J. Jung, *Sci. Rep.*, 2012, **2**, 773.

4 Z. Niu, W. Zhou, J. Chen, G. Feng, H. Li, Y. Hu, W. Ma, H. Dong, J. Li, S. Xie, *Small*, 2013, **9**, 518.

5 T. Qiu, B. Luo, M. Giersig, E. M. Akinoglu, L. Hao, X. Wang, L. Shi, M. Jin, L. Zhi, *Small*, 2014, **10**, 4136.

6 N. Li, G. Yang, Y. Sun, H. Song, H. Cui, G. Yang, C. Wang, *Nano Lett.*, 2015**, 15**, 3195.

7 T. Cheng, Y. Z. Zhang, J. D. Zhang, W. Y. Lai, W. Huang, *J. Mater. Chem. A*, 2016**, 4**, 10493.

8 C. Zhang, T. M. Higgins, S.-H. Park, S. E. O, D. Long, J. N. Coleman, V. Nicolosi, *Nano Energy*, 2016, **28**, 495.

9 N. Li, X. Huang, H. Zhang, Z. Shi, C. Wang, *J. Mater. Chem. A*, 2017, **5**, 16803.

10 H. Moon, H. Lee, J. Kwon, Y.D. Suh, D.K. Kim, I. Ha, J. Yeo, S. Hong, S.H. Ko, *Sci. Rep.,* 2017, **7**, 41981.

11 T. M. Higgins, J. N. Coleman, *ACS Appl. Mater. Interfaces*, 2015, **7**, 16495.

12 K. Lee, H. Lee, Y. Shin, Y. Yoon, D. Kim, H. Lee, *Nano Energy*, 2016, **26**, 746.

13 C. Zhang, B. Anasori, A. S.-Ascaso, S-H. Park,N. McEvoy, A. Shmeliov, G. S. Duesberg, J. N. Coleman, Y. Gogotsi, and V. Nicolosi, *Adv. Mater.*, 2017, **29**, 1702678.

14 J. L. Xu, Y. H Liu, X. Gao, Y. Sun, S. Shen, X. Cai, L. Chen, and S.D. Wang, *ACS Appl. Mater. Interfaces*, 2017, **9,** 27649.

15 Y.-H. Liu, J.-L. Xu, S. Shen, X.-L. Cai, L.-S. Chena and S.-D. Wang, *J. Mater. Chem. A,* 2017, **5**, 9032.

16 T. Cheng, Y. Z. Zhang, J-P. Yi, L. Yang, J-D. Zhang, W. Y. Lai, W. Huang, *J. Mater. Chem. A*, 2016, **4**, 13754.

17 Y.-H. Liu, J.-L. Xu, X. Gao, Y.-L. Sun, J.-J. Lv, S. Shen, L.-S. Chen and S.-D. Wang, *Energy Environ. Sci.*, 2017, **10**, 2534.

18 X. Liu, D. Li, X. Chen, W-Y. Lai, W. Huang, *ACS Appl. Mater. Interfaces*, 2018, **10**, 32536.

19 S. B. Singh, T. Kshetria, Th. I. Singh, N. H. Kim, J. H. Lee, *Chemical Engineering Journal*, 2019, **359**, 197.

20 X. Liu, Y. Gao, G. Yang, *Nanoscale,* 2016, **8**, 4227.

21 P. Chen, G. Shen, *Appl. Phys. Lett*., 2009, **94**, 043113 1.

22 Y. Wang, W. Zhou, Q. Kang, J. Chen, Y. Li, X. Feng, D. Wang, Y. Ma, and W. Huang, *ACS Appl. Mater. Interfaces,* 2018, **10**, 27001.

23 R. T. Gintinga, M. M. Ovhala, J-W. Kang, *Nano Energy,* 2018, **53**, 650–657

24 N. Li, X. Huang, H. Zhang, *J. Alloy. Compd*., 2017, **712**, 194.

25 F. Chen, P. Wan, H. Xu, X. Sun, *ACS Appl. Mater. Interfaces,* 2017, **9**, 17865.

26 J. J. Yoo, K. Balakrishnan, J. Huang, V. Meunier, B.G. Sumpter, A. Srivastava, M. Conway, A.L. Mohana Reddy, J. Yu, R. Vajtai, P.M. Ajayan, *Nano Lett.,* 2011, **11**, 1423.